Methylene Blue Adsorption by Magnesium Oxide Nanoparticles Immobilized with Chitosan (CS-MgONP): Response Surface Methodology, Isotherm, Kinetics and Thermodynamic Studies

Myneni, Venkata Ratnam*[+]

Department of Chemical Engineering, Erode Sengunthar Engineering College, Tamil Nadu, INDIA

Kanidarapu, Nagamalleswara Rao

CDMM, Vellore Institute of Technology, Vellore, Tamil Nadu, INDIA

Vangalapati, Meena

Department of Chemical Engineering, A.U. College of Engineering, Vizag, A.P, INDIA

ABSTRACT: *In this research, a chitosan-immobilized magnesium oxide nanoparticle (CS-MgONP) was synthesized to evaluate it as a prospective adsorbent for a cationic Methylene Blue (MB) dye. For the synthesized adsorbent, functional groups were analyzed through Fourier transform InfraRed (FT-IR) spectroscopy. X-Ray Diffraction (XRD) and Scanning Electron Microscopy (SEM) were used to identify the structural and morphological observations. The evaluation of process parameters such as pH (5-9), CS-MgONP dosage (0.2-0.6g/L), initial MB concentration (10-30mg/L), and temperature (283-323K) on MB adsorption was done at an equilibrium agitation time of 70 min using Central Composite Design (CCD) of Response Surface Methodology (RSM). MB removal percentage of 94.51% (desirability=0.829) was obtained under the optimal conditions of pH=7.28, dosage=0.47g/L, initial MB concentration= 19.37mg/L and temperature =309.76K. The adsorption onto CS-MgONP fits well with pseudo-second-order kinetics equation and equilibrium data made the best fit with Langmuir isotherm with maximum MB uptake capacity of 163.87mg/g.*

KEYWORDS: *Magnesium oxide nanoparticles; Chitosan; Dyes, Nano-adsorbents; Kinetics; Equilibrium.*

INTRODUCTION

Due to the enormous quantities of industrial effluents released as a consequence of rapid industrialization, the environment is at considerable risk [1,2]. Major contributors to colored effluents are textiles, dying, printing, leather, food, cosmetics and paper industries, which are making extensive use of dyes [3]. Wastewaters from these industries are quite lethal and have genuine consequences for people causing cancer and mutagenic

***** *To whom correspondence should be addressed.*
+ E-mail: *mvratnam81@gmail.com*
1021-9986/2020/6/29-42 *14/$/6.04*

effects [4]. Dye particles are stable and in normal conditions do not break down effectively. Therefore, before releasing processed water into sewage, it is important to remove coloring. Numerous techniques, including adsorption, chemical coagulation, biological degradation, and oxidation, have been used to treat dye effluents these day[1,5]. Chemical and biological methods that will be used for color removal are technically complex and costly. Adsorption is an effective and promising color removal method from wastewater [6]. Methylene blue (MB, $C_{16}H_{18}N_3SCl$) is a cationic dye considered as a model pollutant due to the complex structure and high non-biodegradability. Exposure of higher levels of MB (>2ppm) may cause eye burns, leading to permanent eye injury [7,8]. MB will be used in textile, leather, pulp and paper industries.

Because of their superior characteristics, metal oxide nanoparticles have been widely researched for their environmental and energy applications. Among various nano-metal oxides, nano-sized magnesium has proven to be a destructive adsorbent for treating various gaseous pollutants and often receiving significant consideration for wastewater decontamination [9,10]. Low magnesium oxide costs, outstanding chemical stability, higher surface area and non-toxicity are the primary reasons for this improved attention [11]. Although nano-MgO efficiently removes anionic dyes, there is little study of their adsorption effectiveness against cationic dyes [12].

The natural high molecular weight polymer Chitosan (CS) attracted significant interest with its non-toxicity, antibacterial activity and biocompatibility [13]. Chitosan has an excellent binding capacity of pollutants on the surface by means of hydroxyl (-OH) and amino ($-NH_2$) groups, making it an effective adsorbent with a high dye removal capacity [14, 15]. However, the greater solubility of Chitosan with many organic acids, poor mechanical strength, and small surface area limit its application in waste water treatment. Several researchers have been exploring chemical modifications such as cross-linking to enhance the mechanical and physiochemical characteristics [16]. Recent studies have shown that nanocomposites formation is a good way to obtain improvements in the specified properties. Because of the strong interaction between chitosan and nano particles [17], chitosan-based nanocomposites have shown great capacity to remove pollutants. *Haldorai et al.* [18] synthesized chitosan-immobilized magnesium nanoparticles. The synthesized composite demonstrates excellent removal of dye in the case of methyl orange and also displays antibacterial characteristics. *Travolu et al.* [19] functionalized Graphite Oxide (GO) with magnetic chitosan, with a higher adsorption capacity of 425mg/g for reactive black adsorption. The chitosan obtained from shrimp shells treated by impregnation with granular activated carbon used as an adsorbent to remove MB. *Dehagi et al.* [20] synthesized chitosan-ZnO nanoparticles with superb adsorption performance to remove pesticides with extremely good regeneration capability. The chitosan-Al_2O_3-iron oxide composite adsorbent has been prepared to remove methyl orange reveals a strong adsorption ability of 417mg/g[21].

Design of experiments (DOE) will assist us in conducting acceptable optimal experimental runs and for studying the interaction and relationship between variables [22]. Response Surface Methodology (RSM) is an appropriate modeling and optimization method that utilizes quantitative data from suitable designed trials to determine working conditions [23]. The present work aims to prepare a composite for the MB removal using magnesium oxide nanoparticles and chitosan and to develop a model to predict the optimum operating conditions relying on the experimental findings. Central Composite Design (CCD) was used to evaluate the effects of pH, CS-MgONP dosage; MB concentration and temperature on the adsorption efficiency were examined by using batch experiments. Kinetics, isotherm and thermodynamic tests were also performed. The adsorption mechanism was evaluated using the kinetic parameters. To determine the correlation between isotherm models and experimental information, the Langmuir, Freundlich, Temkin and Redlich-Peterson (R-P) models were employed. CS-MgONP morphology was evaluated using Scanning Electron Microscopy (SEM). Also, the structural and functional groups were determined by X-Ray Diffraction (XRD), and Fourier Transform InfraRed (FT-IR) spectroscopy.

EXPERIMENTAL SECTION

Chemicals & Reagents

Magnesium Nitrate GR (Mg $(NO_3)_2.6H_2O$) procured from Merck Chemicals. Chitosan with a high degree of acetylation (>86%), with molecular weight of 2.6×10^5,

Polyvinylpyrrolidone (PVP) & ammonium hydroxide (NH_4OH) were purchased from Loba Chemie Pvt. Ltd. (India). Glacial Acetic acid, NaOH was obtained from Fisher Scientific. Double distilled water was used to prepare all the solutions. The pH adjustments were carried out by the addition of 0.1N HCl or 0.1N NaOH.

Synthesis of adsorbent:

The synthesis procedure used in the current study was adopted from haldorai et.al(18). MgO nanoparticles were produced with PVP as a stabilizer and ammonium hydroxide as a precipitating agent by chemical precipitation of Mg $(NO_3)_2.6H_2O$. 1g of chitosan flakes dissolved in a 50mL acetic acid solution of 1% (v/v) and stirred at 50°C and 500rpm overnight until a clear solution was obtained. In order to remove the insoluble chitosan flakes, the solution was further filtrated. To this, 1g of MgO nanoparticles dispersed in 50mL of 1% (v/v) acetic acid were added and continuously stirred until a homogeneous clear solution was obtained. 0.1N NaOH was then added drop-wise until the pH value of 10 was reached by the solution. The resulting precipitate was heated for 5h at 80^0C and then rinsed and filtered extensively with distilled water to remove any residual NaOH and dried overnight at 60^0C. The synthesized composite was labeled CS-MgONP and was used in adsorption experiments.

Characterization of adsorbent

Field emission scanning electron microscopy (FE-SEM Carl Zeiss NTS GmbH, Germany) was employed for the study of the size and morphology of synthesized MgONP and CS-MgONP. The studies of X-ray diffraction were performed using X-ray diffractometer regaku, in the 2θ range of 10-80 degrees, Cu-Kα radiation (λ=1.5418 A°) is used with a scan rate of 0.05^o s^{-1}. The unused and used adsorbent samples FT-IR spectra were recorded using the 4000-400 cm^{-1} Bruker alpha FT-IR spectrometer.

Adsorption Experimentation and Statistical Analysis

50mL of an aqueous solution (containing a specified initial dye concentration) is taken in a conical flask of 250mL for adsorption experiments. In an orbital shaker at room temperature (303K), a certain quantity of adsorbent is added to the aqueous solution and agitated. Similarly,

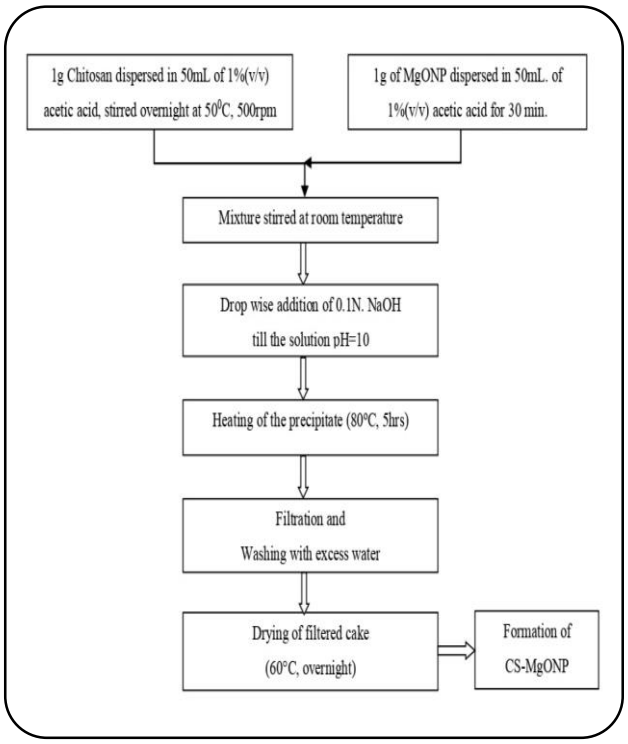

Fig. 1: Synthesis Procedure for CS-MgONP.

more samples with varying parameters are prepared in conical flasks. The samples after adsorption are filtered separately by whatman grade 42 filter paper and analyzed for residual dye concentrations in UV-absorption spectra. The percentage of dye adsorption is calculated as (C_0-C_e) $x100/C_0$ where C_0 is the initial dye concentration in aqueous solution and C_e is the equilibrium concentration of dye in aqueous solution(24).

RSM is a set of mathematical and statistical methods based on the fitting the experimental information with a polynomial equation [25]. The goal is to simultaneously optimize the levels of these process variables in order to achieve the best system performance. The process of optimization includes three major steps: conducting the experimentation that is statistically designed, quantifying the coefficients in a mathematical model and making predictions about the response as well as checking the adequacy of the model. To optimize process parameters in adsorption studies, CCD can be applied with great confidence [26, 27]. The full CCD consists primarily of (1) a full 2n factorial design (n = number of test variables) (2) n_0 center points ($n_0 \geq 1$) and (3) two axial points on the axis of each design variable at a distance of 2n/4 from the design center. Hence, the total number of design points,

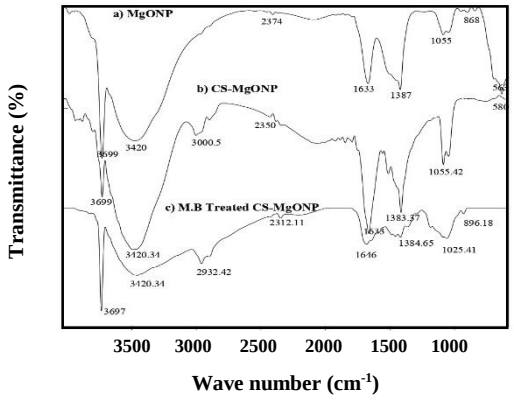

Fig. 2: FT-IR spectrum of (a) MgONP (b) CS-MgONP (c) MB treated CS-MgONP.

$N = 2n + 2n + n_0$ and the five levels of the variables are (–2n/4, –1, 0, +1, +2n/4).

RESULTS AND DISCUSSION

Characterization of adsorbent

Fig. 2 is the FTIR measurement of MgONP, CS-MgONP and CS-MgONP treated by MB. In Fig.2(a), the bands below 1000cm^{-1} indicates the presence of Mg-O bonds. The band at 1055cm^{-1} might be because of the stretching vibrations of C-O-C. In Fig. 2(b), the expanded band at 1638cm^{-1} confirms the presence of amide group indicating the presence of chitosan. The asymmetric and symmetric stretching COO- vibrations were observed at 1383cm^{-1}. A small narrow band around 2350cm^{-1} confirms the presence of CO_2 absorbed by magnesium oxide. The band at 3000 cm^{-1} denote the presence of stretching C – H vibrations in CH_2 or C = C – H group. The narrow bands at 3420cm^{-1} and 3699cm^{-1} were due to stretching vibrations correspondingly of physically adsorbed H_2O molecules as well as surface -OH groups, -NH_2 strongly disturbed by hydrogen bonding. When compared with Fig.2 (b), the spectrum changes observed in Fig. 2(c) at 3699cm^{-1} indicates that -OH groups were one of the functional groups responsible for adsorption [28]. Apart from -OH groups, the functional group present at 1663cm^{-1} i.e. N–H (amide) bending vibrations are probably another functional group responsible for MB adsorption.

Fig. 3 (a) shows the XRD pattern of chitosan immobilized magnesium nanoparticles (CS-MgONP). Both chitosan, MgO peaks have been identified in the synthesized composite. The peak at 20^0 reflects chitosan, and the peaks at 38^0, 62^0 and 74^0 reflect the MgO. From other peaks at 50^0 and 58^0, a small amount of MgO hydration into Mg $(OH)_2$ was evident. The SEM image (Fig.3 (b)) showed the successful chitosan immobilization onto MgO. The nanoparticles of magnesium retain their nanostructure while strengthening the matrix of chitosan. Chitosan-MgO interaction enhanced the properties of composite CS–MgO.

Effect of agitation time:

The effect of agitation time has been an essential factor in the sorption experiments as the data will enable confirmation of the duration of agitation to achieve the adsorption process equilibrium [29]. MgO nanoparticles could quickly adsorb dyes, achieving equilibrium in very short time, with very high capacity for adsorption [30]. MB's adsorption was examined with agitation time varying from 5 to 120 min. At a concentration of 20mg/L and a dosage of 0.2g/L, the rapid adsorption capacity of CS-MgONP adsorbent is indicated by 60.25% of MB adsorption with in the first 5 minutes. The percentage of adsorption within 70 minutes reaches up to 85.6 percent, later remains constant, indicating the achievement of equilibrium. In the present study, the adsorption rate of MB was very fast in the initial stages from 5min to 30min and stable at 70minutes of agitation time, which can be attributed to the availability of active sites on CS-MgONP and as time goes by, the saturation of active sites with the dye molecules occurs and therefore the adsorption slows down and the adsorbent's capacity was found to be constant. Consequently, the effect of other parameters on MB's adsorption was studied at a time of 70min.

Experimental design & optimization using Response Surface Methodology (RSM)

A four-factor CCD (Central Composite Design) was used to monitor the effect of variables based on 30 experimental runs at different numerical values of pH (X1), adsorbent dosage (X2), initial dye solution concentration (X3), and temperature (X4) to investigate their main and interaction contribution to dye removal while maintaining agitation time as constant. STATISTICA Version 8.0 (Stat-Ease, Inc) was used for analyzing the response. Variance analysis (ANOVA) was used to carry out diagnostic checking tests based on the Fishers F test for adequacy of the proposed model.

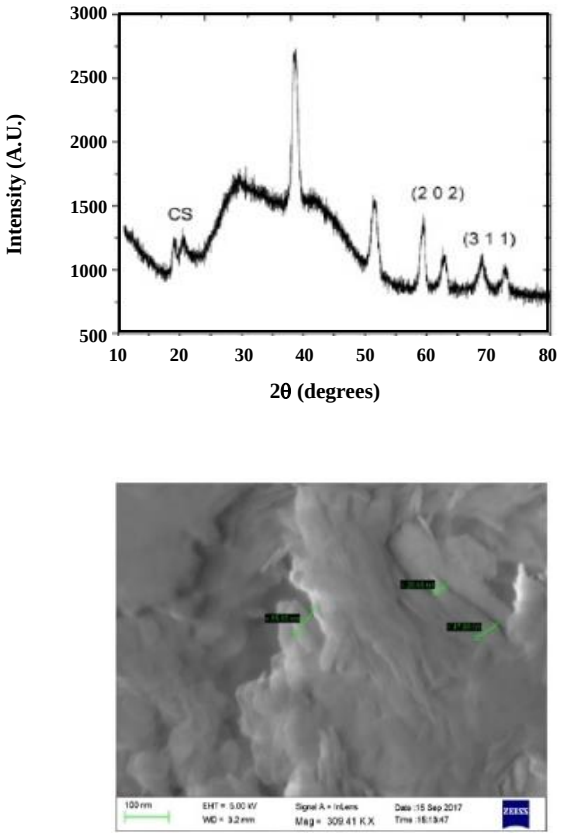

Fig. 3: (a) XRD Image; (b) SEM Image of CS-MgONP.

The coefficient of regression (R^2) shows the amount of variation around the model's mean. Table 1 summarizes the ranges of each studied variable. Table 2 presents the coded and uncoded levels of independent factors corresponding to CCD along with their responses according to 30 experiments. Experimental conditions [Coded Values] and observed response values of central composite design with 2^4 factorial runs, 6- central points and 8- axial points, and accordingly regression and quadratic equation was constructed by means of CCD to correlate relationship among approximation and prediction of responses. Thus, the second-order CCD models with variables obtained for adsorption process were as follows:

Final Equation in Terms of Actual Factors:

% MB Removal = -1789.80615 +42.16667*pH-32.12583*dosage(g/L) -2.42063*concentration(mg/L)+ 11.37493 *Temparature(K)+9.275*pH*dosage+ 0.19575*pH*concentration+0.09*pH*Temparature+0.497*dosage* Temparature+0.015125*concentration *Temparature-5.36792*pH^2-202.79167*$dosage^2$-0.095267*$concentration^2$ -0.020267*$Temparature^2$

Analysis of variance (ANOVA):

Table 3 presents the variance analysis corresponding to experimental results. The low probability (< 0.05) of 302.03 F-value implied the accuracy of the model. Furthermore, the acceptable and reasonable value of the lack of fit with F-value of 0.7022 with probability (> 0.05) indicates that the method is suitable for the proper presentation of experimental data. The model shows the high R^2 value of 0.9959 for MB removal indicates that a good agreement existed between the experimental and predicted results. The predicted value of R^2 was also 0.9852, which was in reasonable agreement with the adjusted value of R^2 of 0.9926. Appropriate accuracy (signal to noise ratio) of the model was found to be 63.374, which indicates an adequate signal and demonstrates that this model can be used to navigate the design space. Fig. 4 showed that predicted value of the responses from model was in agreement with observed values over the selected range of independent variables with reasonable higher values of coefficient of determination (R^2)

Response surface plots and interactions between the adsorption parameters for MB adsorption

The response surface 3D contour plots of percentage adsorption of MB vs. the interactive effects of pH, initial MB concentration, adsorbent dosage and temperature of the aqueous solution were shown in Fig 5(a) – 5(e). Each contour plot represents a number of combinations of two test parameters with the other parameter maintained at zero levels. The surface confined in the smallest curve (circular or elliptical) of the contour plot indicated the maximum percentage adsorption of MB. The experimental results indicate that MB adsorption increased with higher solution pH and higher dosage [Fig. 5 (a)]. The efficiency of adsorption increased and then remained almost constant with a dosage range of 0.3–0.4g/L and 0.4–0.5g/L respectively at pH > 7.0, the transfer of an excess proton to the reactive center led to the appearance of more repulsive electrostatic forces and a decrease in the percentage of removal. From the pH values 4.0-7.0, MB molecules showed strong attractive forces with the adsorbent surface causing more reactive centers to be generated as well as more accumulation mechanisms such as hydrogen bonding, vander-waals interaction and electrostatic attraction forces. Therefore, the removal percentage reaches its maximum pH 7.0. As illustrated

Table 1: Levels of process variables in coded and un-coded form for % adsorption of MB by CS-MgONP.

Variable	Name of the Process Variable	Range and levels				
		-2	-1	0	1	2
X_1	pH of aqueous solution	5	6	7	8	9
X_2	adsorbent dosage, w, g/L	0.2	0.3	0.4	0.5	0.6
X_3	Initial concentration of MB in aqueous solution, C_o, mg/L	10	15	20	25	30
X_4	Temperature, T, K	283	293	303	313	323

Table 2: Results from CCD for MB adsorption by CS-MgONP.

Run no.	X_1, pH	X_2, w	X_3, C_0	X_4, T	% adsorption of MB	
					Experimental	Predicted
1	7.00	0.40	20.00	303.00	92.8	92.68
2	8.00	0.50	25.00	313.00	90.1	89.83
3	7.00	0.40	20.00	323.00	89.46	89.07
4	7.00	0.40	20.00	283.00	80.56	80.08
5	7.00	0.40	20.00	303.00	92.34	92.68
6	7.00	0.60	20.00	303.00	89.12	88.83
7	6.00	0.50	15.00	293.00	81.3	81.45
8	7.00	0.40	10.00	303.00	86.38	85.93
9	5.00	0.40	20.00	303.00	67.92	67.39
10	8.00	0.30	15.00	313.00	81.8	82.03
11	8.00	0.50	15.00	293.00	83.16	83.37
12	7.00	0.40	20.00	303.00	91.93	92.68
13	6.00	0.30	25.00	293.00	73.6	73.78
14	8.00	0.30	25.00	313.00	82.32	82.72
15	8.00	0.50	15.00	313.00	88.78	89.15
16	8.00	0.50	25.00	293.00	80.7	81.03
17	6.00	0.30	15.00	313.00	80.47	80.22
18	7.00	0.40	20.00	303.00	93.6	92.68
19	6.00	0.50	25.00	293.00	75.1	75.20
20	6.00	0.50	15.00	313.00	83.14	83.63
21	6.00	0.50	25.00	313.00	80.3	80.40
22	6.00	0.30	25.00	313.00	76.41	77.00
23	7.00	0.40	20.00	303.00	92.16	92.68
24	6.00	0.30	15.00	293.00	79.44	80.04
25	8.00	0.30	25.00	293.00	75.6	75.91
26	7.00	0.20	20.00	303.00	80.89	80.31
27	9.00	0.40	20.00	303.00	75.37	75.03
28	7.00	0.40	30.00	303.00	80.8	80.37
29	7.00	0.40	20.00	303.00	93.24	92.68
30	8.00	0.30	15.00	293.00	78.26	78.24

Table 3: ANOVA Table for model to predict % removal of MB by CS-MgONP using CCD.

Source	Sum of Squares	df	Mean Square	F Value	p-value
Model	1340.24	13	103.1	302.03	< 0.0001
X_1-pH	87.63	1	87.63	256.73	< 0.0001
X_2-dosage	108.97	1	108.97	319.24	< 0.0001
X_3-Conc.	46.43	1	46.43	136.01	< 0.0001
X_4-Temp	121.32	1	121.32	355.42	< 0.0001
X_1X_2	13.76	1	13.76	40.32	< 0.0001
X_1X_3	15.33	1	15.33	44.9	< 0.0001
X_1X_4	12.96	1	12.96	37.97	< 0.0001
X_2X_4	3.96	1	3.96	11.6	0.0036
X_3X_4	9.15	1	9.15	26.81	< 0.0001
X_1^2	790.34	1	790.34	2315.4	< 0.0001
X_2^2	112.8	1	112.8	330.46	< 0.0001
X_3^2	155.58	1	155.58	455.8	< 0.0001
X_4^2	112.66	1	112.66	330.05	< 0.0001
Residual	5.46	16	0.34		
Lack of Fit	3.34	11	0.3	0.71	0.7022
Pure Error	2.12	5	0.42		
Cor Total	1345.7	29			

df- degree of freedom; SS- sum of squares; F- factor F; P- probability

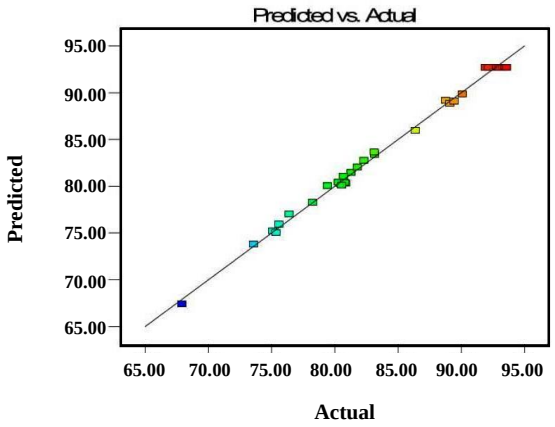

Fig. 4: Comparison plot between the experimental and predicted data for adsorption of MB onto CS-MgONP.

in Fig. 5 (b), at lower initial dye concentration, the maximum removal percentage was observed. Fig. 5 (c) indicates the MB adsorption temperature interaction of the aqueous solution with the pH. Consequently, the efficiency of adsorption increased at higher temperatures. The enhancement in removal percentage with increased dosage at higher temperatures may be related to the high available surface area and vacant site of adsorbents (Fig. 5 (d)). The effect of initial dyes concentration on % MB removal shows that at low concentrations of MB, the % adsorption was higher due to the low solute to adsorbent vacant sites ratio. The decrease in % MB removal at higher concentrations was found to be less at higher temperatures, when compared with % MB removal at lower temperatures (Fig.5 (e)).

Optimization

Fig.6 shows the desirability profile for the percentage of removal of MB versus the variables. The desirability varies from 0.0 to 1.0 corresponds to the approach to the very desirable condition from undesirable. Considering the percentage of removal to be maximized, optimum conditions were obtained to be pH 7.28, dosage 0.47g /L, 19.37mg/L of initial MB concentration at 309.76K.

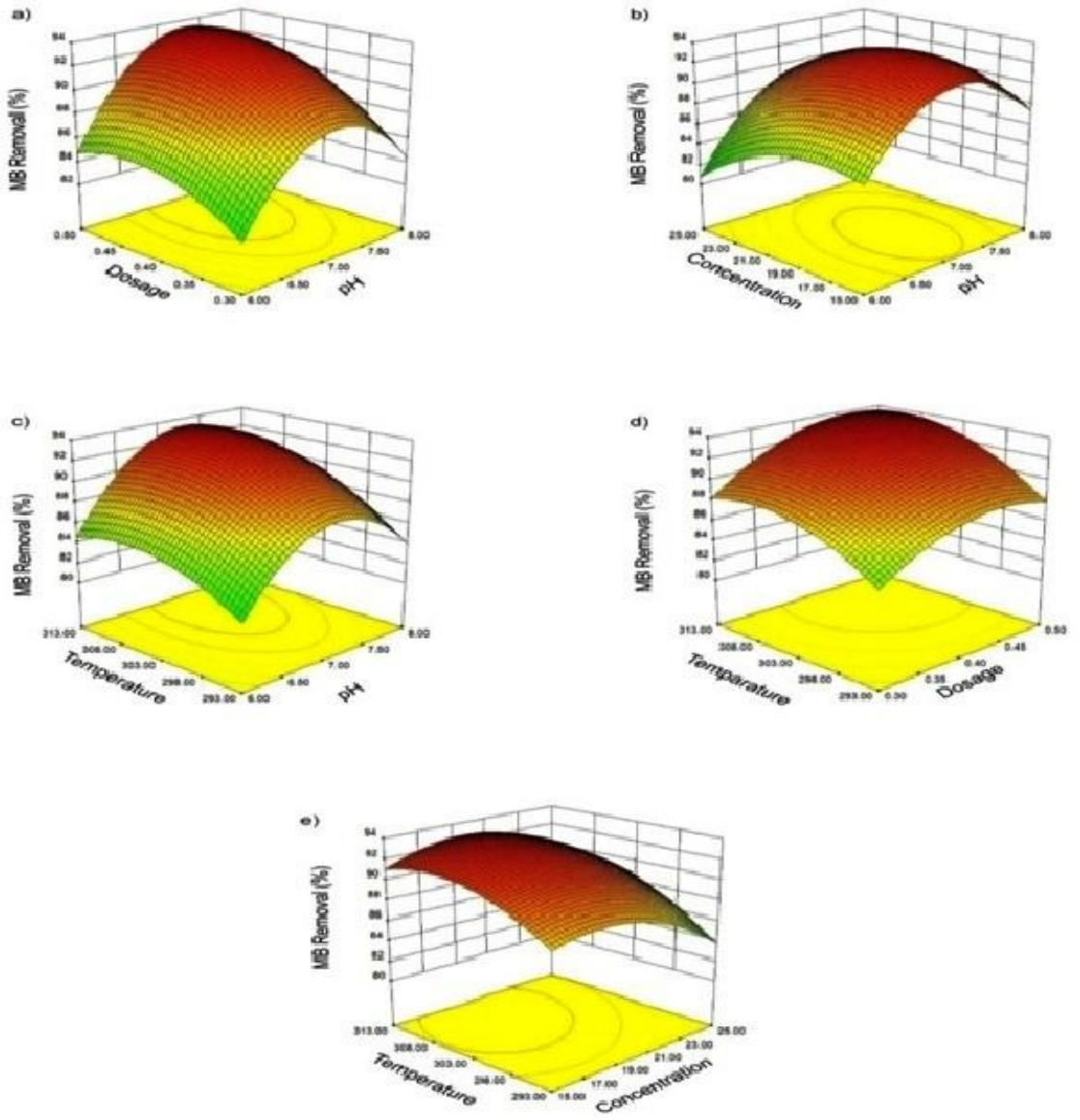

Fig.5: 3D response surface plots for adsorption of MB onto CS-MgONP- Interactive effects of (a) pH and Dosage (b) pH and Concentration (c) pH and Temperature (d) Dosage and Temperature (e) Concentration and Temperature

The 94.51 percent removal percentage was obtained with a total desirability of 0.829.

Adsorption Kinetics

For the kinetic study, the effect of contact time on MB adsorption was investigated at an initial concentration of MB 20mg/L at pH=7 and Temperature= 303K in solutions containing fixed adsorbent amounts (0.4g/L). Fig. 7 (a) represents non-linear fitting of experimental kinetics with Pseudo-First Order (PFO), Pseudo-Second Order (PSO) and Elovich models. Table 4 presents the coefficients of regression (R^2, χ^2) along with the kinetic constants. The inapplicability of the pseudo-first-order model for experimental data representation was confirmed by the difference between calculated (q_e, cal) and experimental (q_e, exp) values and their lower coefficient of correlation. Pseudo-second order kinetics best describes the kinetics of CS-MgONP adsorbent MB adsorption, which was evident

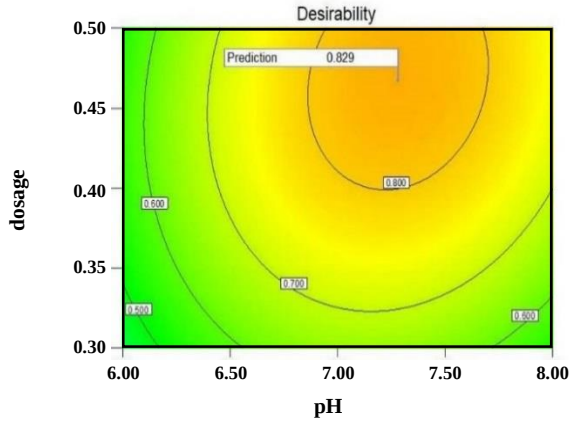

Fig. 6: Desirability Plot for MB Adsorption onto CS-MgONP.

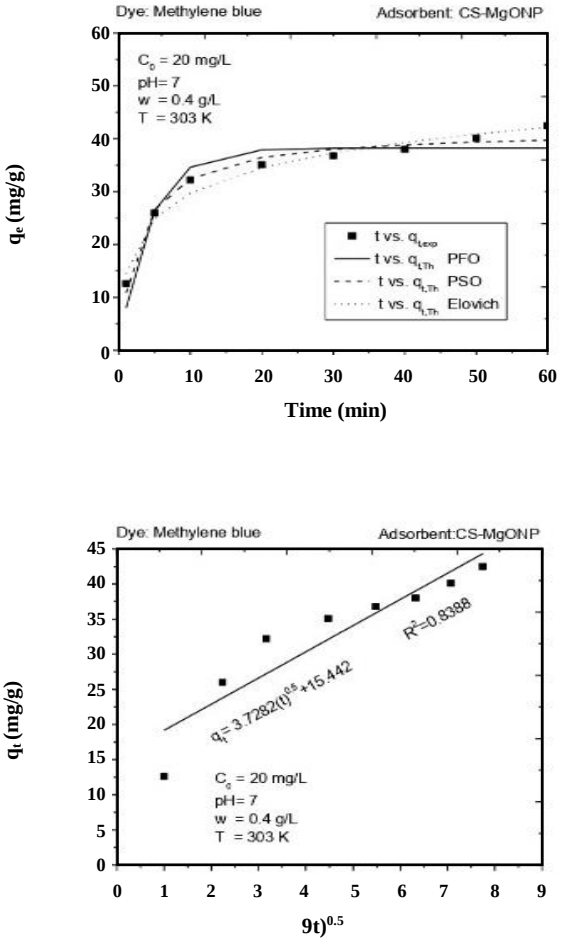

Fig. 7: Kinetic studies for adsorption of MB onto CS-MgONP (a) PFO, PSO and Elovich (b) IPD models.

from high values of R^2 and low levels of χ^2[31]. The high values for the linear regression coefficient ($R^2 > 0.979$) show the suitability of the Elovich model for the best representation of data corresponding to the present adsorption system and also the contribution of chemisorptions (chemical reaction) to the current adsorption mechanism, particularly in the kinetic region. If the plot of q_t versus $t^{0.5}$ gives a straight line, passing through the origin, then intra-particle diffusion becomes a rate-limiting step, according to the intra-particle diffusion model. From Fig. 7(b), it was identified that the relationship between q^t and $t^{0.5}$ was not linear over a whole time range in the present study, indicating that the adsorption is affected by several processes. Intercept values give an idea of the thickness of the boundary layer, i.e. the larger intercept the greater would be the effect of the boundary layer and this means that more boundary layer is controlled by the adsorption. R_i value (0.6366) between 0.5-0.9 indicates the process of adsorption is the initial process of adsorption.

Equilibrium

Studies show that linear regression may not be a suitable technique for predicting the optimum isotherm as the linearization of experimental data can sometimes distort the isothermic error distribution structure [36,37]. Linearization problems can be avoided if the isotherms were fitted by nonlinear regression method to the experimental data. Non-linear isotherm regression was performed here and results were compared with linear regression results. Table 5 presents the isotherm constants & regression parameters (R^2, χ^2). The three parameter R-P isotherm was better equipped with non-linear regression instead of the linear fitting trail & error procedure. Based on R^2 values, the Langmuir isotherm's linear form has more efficiency in representing and explaining adsorption data, i.e. adsorption is limited to monolayer coverage and the surface is relatively homogeneous in functional groups with significant interaction with dye molecules. CS-MgONP adsorbent maximum adsorption capacity (q_{max}) of MB was 163.87. Based on the R_L values calculated from Langmuir constant k_L, which were in the ranges of 0.0638-0.405 ($0<R_L<1$), the adsorption process could be assessed as beneficial(5). The value for Freundlich constant (n) of 0.3746 (between 0 and 1), which was considered the adsorption intensity factor indicating favourable adsorption.

Table 4: Kinetic parameters& their correlation coefficients calculated using Non-Linear Regression Analysis fo.r the adsorption of MB onto CS-MgONP (pH=7; dosage= 0.4g/L; Concentration =20mg/L; Temperature=303K)

Dye-Methylene Blue		Adsorbent:CS-MgONP	
Model	Equation	Parameters	Values
Pseudo-First order[32] $q_t = q_e(1 - e^{-k_1 t})$	Where q_e & q_t are the amount of dye adsorbed at the equilibrium & at a time't'; k_1 is the overall rate constant of pseudo-first order adsorption.	$k_1(min^{-1})$	0.2357
		q_e(calc)mg/g	38.263
		R^2	0.9101
		χ^2	3.596
Pseudo-Second order[33] $q_t = \frac{q_e^2 k_2 t}{1 + q_e k_2 t}$	k_2 is the second order rate constant.	k_2(g/(mg-min)	0.00851
		q_e(calc) mg/g	41.6176
		R^2	0.9759
		χ^2	0.599
Elovich [34] $q_t = \frac{\ln(1 + \alpha\beta t)}{\beta}$	α is initial sorption rate constant. β is related to extent of surface coverage and activation energy for chemisorptions.	β(g/mg)	0.1432
		α (mg/g.min)	48.711
		R^2	0.9791
		χ^2	0.5738
Intra-particle diffusion[35] $q_t = k_{diff} t^{0.5} + C$	k_{diff} is intra-particle diffusion rate constant. C is thickness of the boundary layer	$K_{diff}(mg/g.min^{-1/2})$	3.7281
		C(mg/g)	15.442
		R_i	0.6366
		R^2	0.8618
		χ^2	3.8388
		q_e(Exp.)mg/g	44.35

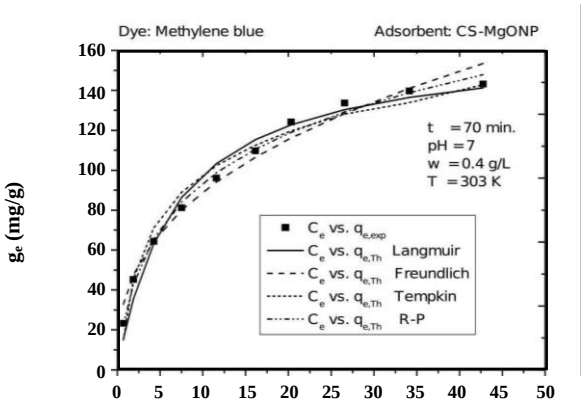

Fig. 8: Isotherm plots for adsorption of MB onto CS-MgONP.

Temkin isotherm contains a factor that species-adsorbent interactions are explicitly accounted for. Sorption heat (b) was 81.36 J/mol, whereas the binding constant of equilibrium (K_T) was 2.314 L/mg. The Redlich-Peterson (R-P) isotherm model will be used for representing adsorption equilibrium over a wide concentration range and can be applied in either homogeneous or heterogeneous system due to its versatility. The constant of R-P isotherm 'g' value which lies in between 0 and 1 (0.78) indicates that the model was approaching Langmuir isotherm.

Thermodynamics

Thermodynamics parameters (energy and entropy) are used to determine the spontaneity of an adsorption process. The changes in Gibbs free energy (ΔG^0), enthalpy (ΔH^0) and entropy (ΔS^0) of adsorption process were determined. Equilibrium constants at different temperatures were evaluated by plotting $\ln(C_S/C_e)$ vs. C_e and extrapolating C_e to Zero[42].

where

C_S = concentration of adsorbate adsorbed on to the adsorbent = $C_0 - C_e$

Table 5: Isotherm constants & their correlation coefficients calculated using Non-Linear Regression Analysis for the adsorption of MB onto CS-MgONP (Agitation time = 70min., pH=7; dosage= 0.4g/L; Temperature=303K).

Dye: Methylene Blue		Adsorbent:CS-MgONP	
Model	Equation	Parameters	Value of parameters
Langmuir [38] $q_e = \frac{q_{max} k_L C_e}{(1 + k_L C_e)}$	Where q_e is the amount of dye adsorbed at the equilibrium and q_{max} is the maximum monolayer adsorption capacity. C_e is equilibrium dye concentration. K_L is the Langmuir constant related to free energy of adsorption	q_{max}(mg/g)	163.87
		k_L(L/ mg)	0.147
		R_L	0.0638-0.405
		R^2	0.981
		χ^2	8.189
Freundlich [39] $q_e = K_F C_e^n$	Where K_F is the Freundlich constant and n is an indicator of favorability of adsorption.	n	0.3746
		K_F (mg/g)/(mg/L)^n	37.571
		R^2	0.979
		χ^2	4.5615
Temkin[40] $q_e = B \ln(C_e K_T)$	B= RT/b; R is universal gas constant =8.314 J.K^{-1}.mol^{-1}; T is absolute temperature in K; b is heat of sorption in J.mol^{-1}; K_T is equilibrium binding capacity	B	31.099
		K_T(L/mg)	2.314
		R^2	0.98
		χ^2	6.9986
Redlich-Peterson[41] $q_e = \frac{k_{rp} C_e}{(1 + a_{rp} C_e^g)}$	k_{rp} and a_{rp} are the Redlich-Peterson constants and g (dimensionless) is an exponent whose value must lie between 0 and 1.	k_{rp} (L/g)	49.236
		a_{rp} ((mg/L)$^{-g}$	0.7052
		g	0.78082
		R^2	0.9938
		χ^2	0.9151

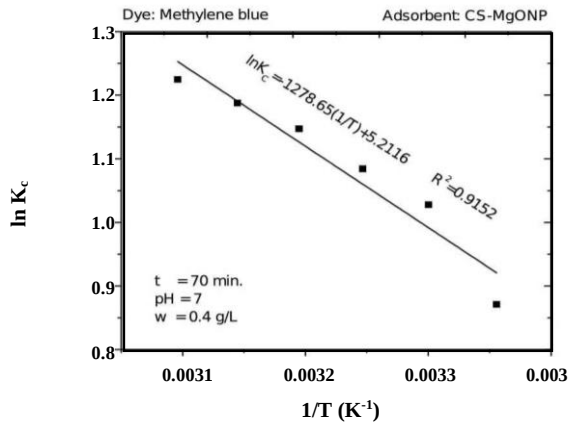

Fig. 9: Van't Hoffs Thermodynamic plot for adsorption of MB onto CS-MgONP.

C_e = concentration of adsorbate in solution at equilibrium

C_0 = initial concentration of adsorbate in solution.

As a function of 1/T, Van't Hoff's ln K_C plot yields a straight line as shown in Fig. 9 from which upper and lower slope0 and lower slope0 were calculated. The negative values of ΔG^0 at different temperatures (Table 6) indicate that MB adsorption is a spontaneous process, and at higher temperatures the adsorbent used in this study has higher affinity. The positive value of the ΔH^0 indicates the adsorption's endothermic nature. The positive value of ΔS^0 suggests that randomness on the solid / solution interface increases with MB's adsorption on the CS-MgONP adsorbent.

CONCLUSIONS

The objective of the current work is to evaluate and optimize

Table 6: Thermodynamic parameters for adsorption of MB by CS-MgONP.

Temperature (K)	Equilibrium Constant (K_C)	ΔG^o (K.J/mol)	ΔH^o (J/mol.K)	ΔS^o (J/mol.K)	Vant Hoff Equation
298	2.389	-2.1577	10.625	43.324	$\ln K_C$=-1278.65(1/T)+5.211 R^2= 0.9152
303	2.795	-2.5893			
308	2.957	-2.7762			
313	3.149	-2.9850			
318	3.279	-3.1396			
323	3.403	-3.2887			

the suitability of magnesium oxide nanoparticles immobilized chitosan (CS-MgONP) as an adsorbent for the removal of a cationic dye i.e. methylene blue.

Performance of CS-MgONP on MB removal

- Equilibrium agitation time for adsorption was obtained as 70min. for CS-MgONP
- % MB removal at the optimal variables by CCD-RSM was found to be 94.51% for CS-MgONP
- The experimental kinetics data followed pseudo-second order kinetics & the experimental isotherm data followed Langmuir isotherm.
- The positive values of enthalpy change (ΔH) for the adsorbent indicated an endothermic and irreversible process.
- Adsorption mechanism was identified through FT-IR analysis showed that surface -OH groups, as well as amides (-NH_2) caused the adsorption of MB molecules on to the surface of CS-MgONP.
- The adsorption capacity, which would be considered as a major parameter for evaluating the suitability of adsorbent was obtained as 163.87 mg/g for CS-MgONP.

Received : May 6, 2019 ; Accepted : Sep. 2, 2019

REFERENCES

[1] Hajira T., Atika S., Muhammad S., Synthesis of Kaolin Loaded Ag and Ni Nanocomposites and their Applicability for the Removal of Malachite Green Oxalate Dye, *Iran. J. Chem. Chem. Eng (IJCCE)*, **37(3)**: 11–22 (2018).

[2] Ayub S., Akbar Mohammadi A., Yousefi M., Changani F., Performance Evaluation of Agro-Based Adsorbents for the Removal of Cadmium from Wastewater, *Desalin. Water Treat.*, **142**: 293–299 (2019).

[3] Wang L., Zhang J., And Wang A., Fast Removal of Methylene Blue From Aqueous Solution by Adsorption onto Chitosan-G-Poly (Acrylic Acid)/ Attapulgite Composite, *Desalination*, **266(1-3)**: 33–39 (2011).

[4] J. Ma., F. Yu., L. Zhou., L. Jin., M.X. Yang., J.S. Luan., Y.H. Tang., H.B. Fan., Z.W. Yuan JHC., Enhanced Adsorption Removal of Methyl Orange And Methylene Blue from Aqueous Solution by Alkali-Activated Multiwalled Carbon Nanotubes, *Appl. Mater. Interfaces*, **4(11)**: 5749–5760 (2012).

[5] Mohammadi AA., Alinejad A., Kamarehie B., Javan S., Ghaderpoury A., Ahmadpour M., Metal-Organic Framework Uio-66 for Adsorption of Methylene Blue Dye from Aqueous Solutions, *Int. J. Environ. Sci. Technol.*, **14(9)**: 1959–1968 (2017).

[6] Kamranifar M., Naghizadeh A., Montmorillonite Nanoparticles In Removal of Textile Dyes from Aqueous Solutions: Study of Kinetics and Thermodynamics, *Iran. J. Chem. Chem. Eng. (IJCCE)*, **36(6)**: 127–137 (2017).

[7] Jawad AH., Abd Rashid R., Ismail K., Sabar S., High Surface Area Mesoporous Activated Carbon Developed from Coconut Leaf by Chemical Activation with H_3PO_4 for Adsorption of Methylene Blue, *Desalin. Water Treat.*, **74**: 326–335 (2017).

[8] Jawad AH., Mamat NFH., Abdullah MF., Ismail K., Adsorption of Methylene Blue onto Acid-Treated Mango Peels: Kinetic, Equilibrium and Thermodynamic Study, *Desalin. Water Treat.*, **59**: 210–219 (2017).

[9] Nassar MY., Mohamed TY., Ahmed IS., Samir I., Mgo Nanostructure *via* a Sol-Gel Combustion Synthesis Method Using Different Fuels: An Efficient Nano-Adsorbent for the Removal of Some Anionic Textile Dyes, *J. Mol. Liq.*, **225:** 730-740 (2017).

[10] John Sushma N., Prathyusha D., Swathi G., Madhavi T., Deva Prasad Raju B., Mallikarjuna K., Facile Approach to Synthesize Magnesium Oxide Nanoparticles by Using Clitoria Ternatea—Characterization and *In Vitro* Antioxidant Studies, *Appl. Nanosci.*, **6(3)**: 437–444 (2016).

[11] Purwajanti S., Zhang H., Huang X., Song H., Yang Y., Zhang J., Mesoporous Magnesium Oxide Hollow Spheres as Superior Arsenite Adsorbent: Synthesis and Adsorption Behavior, *ACS Appl. Mater. Interfaces*, **8(38)**: 25306–25312 (2016).

[12] Tan KB., Vakili M., Horri BA., Poh PE., Abdullah AZ., Salamatinia B., Adsorption of Dyes by Nanomaterials: Recent Developments and Adsorption Mechanisms, *Sep. Purif. Technol.* **150**: 229–242 (2015).

[13] Vakili M., Rafatullah M., Salamatinia B., Abdullah AZ., Ibrahim MH., Tan KB.,Gholami Z., Amouzgar P., Application of Chitosan and its Derivatives as Adsorbents for Dye Removal from Water and Wastewater: A Review, *Carbohydr. Polym.*, **113**: 115–130 (2014).

[14] Jawad AH., Mamat NFH., Hameed BH., Ismail K., Biofilm of Cross-Linked Chitosan-Ethylene Glycol Diglycidyl Ether for Removal of Reactive Red 120 and Methyl Orange: Adsorption and Mechanism Studies, *J. Environ. Chem. Eng.*, **7(2)**:102965 (2019).

[15] Hadi Dehghani M., Zarei A., Mesdaghinia A., Nabizadeh R., Alimohammadi M., Afsharnia M., Adsorption of Cr(VI) Ions from Aqueous Systems Using Thermally Sodium Organo-Bentonite Biopolymer Composite (TSOBC): Response Surface Methodology, Isotherm, Kinetic and Thermodynamic Studies, *Desalin. Water Treat.*, **85**: 298–312(2017).

[16] Jawad AH., Azharul Islam M., Hameed BH., Cross-Linked Chitosan Thin Film Coated Onto Glass Plate as an Effective Adsorbent for Adsorption of Reactive Orange 16, *Int. J. Biol. Macromol.*, **95**: 743–749 (2017).

[17] Sanmugam A., Vikraman D., Park H., Kim HS., One-Pot Facile Methodology to Synthesize Chitosan-Zno-Graphene Oxide Hybrid Composites for Better Dye Adsorption and Antibacterial Activity, *Nanomaterials*, **7(11)**: 363 (2017).

[18] Haldorai Y., Shim JJ., An Efficient Removal of Methyl Orange Dye from Aqueous Solution by Adsorption onto Chitosan/Mgo Composite: A Novel Reusable Adsorbent, *Appl. Surf. Sci.*, **292**: 447–453 (2014).

[19] Travlou NA., Kyzas GZ., Lazaridis NK., Deliyanni EA., Functionalization of Graphite Oxide with Magnetic Chitosan for the Preparation of A Nanocomposite Dye Adsorbent, *Langmuir*, **29(5)**: 1657-1668 (2013).

[20] Moradi Dehaghi S., Rahmanifar B., Moradi AM., Azar PA., Removal of Permethrin Pesticide from Water by Chitosan-Zinc Oxide Nanoparticles Composite as an Adsorbent, *J. Saudi Chem. Soc.*, **18(4)**: 348–355 (2014).

[21] Tanhaei B., Ayati A., Lahtinen M., Sillanpaa M., Preparation and Characterization of A Novel Chitosan/Al_2O_3/Magnetite Nanoparticles Composite Adsorbent for Kinetic, Thermodynamic and Isotherm Studies of Methyl Orange Adsorption, *Chem. Eng. J.*, **259**: 1–10 (2015).

[22] Asfaram A., Ghaedi M., Hajati S., Goudarzi A., Dil EA., Screening and Optimization of Highly Effective Ultrasound-Assisted Simultaneous Adsorption of Cationic Dyes onto Mn-Doped Fe_3O_4-Nanoparticle-Loaded Activated Carbon, *Ultrason. Sonochem.*, **34**: 1–12 (2017).

[23] Bagheri AR., Ghaedi M., Asfaram A., Jannesar R., Goudarzi A., Design and Construction of Nanoscale Material for Ultrasonic Assisted Adsorption of Dyes: Application of Derivative Spectrophotometry and Experimental Design Methodology, *Ultrason. Sonochem.*, **35(A)**: 112–123(2017).

[24] Dehghani MH., Zarei A., Mesdaghinia A., Nabizadeh R., Alimohammadi M., Afsharnia M., Mckay G., Production and Application of a Treated Bentonite–Chitosan Composite for the Efficient Removal of Humic Acid from Aqueous Solution, *Chem. Eng. Res. Des.*, **140**:102–115 (2018).

[25] Mohammad AKT., Abdulhameed AS., Jawad AH., Box-Behnken Design to Optimize The Synthesis of New Crosslinked Chitosan-Glyoxal/TiO_2 Nanocomposite: Methyl Orange Adsorption and Mechanism Studies, *Int. J. Biol. Macromol.*, **129**: 98–109 (2019).

[26] Jawad AH., Mohd Ishak MA., Farhan AM., Ismail K., Response Surface Methodology Approach for Optimization of Color Removal and COD Reduction of Methylene Blue Using Microwave-Induced NaOH Activated Carbon from Biomass Waste, *Desalin. Water Treat.*, **62**: 208–220 (2017).

[27] Dehghani MH., Zarei A., Mesdaghinia A., Nabizadeh R., Alimohammadi M., Afsharnia M., Response Surface Modeling, Isotherm, Thermodynamic and Optimization Study of Arsenic (V) Removal from Aqueous Solutions Using Modified Bentonite-Chitosan (MBC), *Korean J. Chem. Eng.*, **34**: 757–767 (2017).

[28] Heidarizad M., Sengor S.S., Synthesis of Graphene Oxide/Magnesium Oxide Nanocomposites with High-Rate Adsorption of Methylene Blue, *J. Mol. Liq.* **224(A)**: 607–617 (2016).

[29] Venkateswarlu P., Ratnam MV., Rao DS., Rao MV., Removal of Chromium from an Aqueous Solution Using Azadirachta Indica (Neem) Leaf Powder as an Adsorbent. *Int. J. Phys. Sci.*, **2(8)**: 188–195 (2007).

[30] Moussavi G., Mahmoudi M., Removal of Azo and Anthraquinone Reactive Dyes from Industrial Wastewaters Using MgO Nanoparticles, *J. Hazard. Mater.*, **168(2-3)**: 806–812 (2009).

[31] Mohan S., Kumar V., Singh DK., Hasan SH., Effective Removal of Lead Ions Using Graphene Oxide-MgO Nanohybrid from Aqueous Solution: Isotherm, Kinetic and Thermodynamic Modeling of Adsorption, *J. Environ. Chem. Eng*., **5(3)**: 2259-2273 (2017).

[32] Lagergren S., Zur Theorie Der Sogenannten Adsorption Gelöster Stoffe, Kungliga Svenska Vetenskapsakademiens, *Handlingar*, **24**(4): 1-39 (1898).

[33] Ho YS., Mckay G., Pseudo-Second Order Model for Sorption Processes, *Process Biochem.*, **34**(5): 451-465(1999).

[34] Mclintock IS., The Elovich Equation in Chemisorption Kinetics, *Nature* **216**: 1204-1205 (1967).

[35] Wu FC., Tseng RL., Juang RS., Initial Behavior of Intraparticle Diffusion Model Used in the Description of Adsorption Kinetics, *Chem. Eng. J*., **153(1-3)**: 1-8 (2009).

[36] Kumar KV., Linear And Non-Linear Regression Analysis For The Sorption Kinetics of Methylene Blue Onto Activated Carbon, *J. Hazard. Mater.*, **137(3)**: 1538–1544 (2006).

[37] Kumar KV., Optimum Sorption Isotherm by Linear and Non-Linear Methods For Malachite Green onto Lemon Peel, *Dye. Pigment.*, **74(3)**: 595–597(2007).

[38] Langmuir I., The Adsorption of Gases on Plane Surfaces of Glass, Mica and Platinum, *J. Am. Chem. Soc.*, **40(9)**: 1361–1403 (1918).

[39] Freundlich H., Über Die Adsorption in Lösungen, *Zeitschrift Für Phys. Chemie*, **57U(1)**: 385-470 (1907).

[40] Aharoni C., Ungarish M., Kinetics of Activated Chemisorption-Part 2.- Theoretical Models, *J. Chem. Soc. Faraday Trans.1*,**73**: 456–464(1977).

[41] Redlich O., Peterson DL., A Useful Adsorption Isotherm, *J. Phys. Chem.*, **63(6)**: 1024–1024 (1959).

[42] Biggar J.W., Cheung M.W., Adsorption of Picloram (4-Amino-3,5,6-Trichloropicolinic Acid) on Panoche, Ephrata, and Palouse Soils: a Thermodynamic Approach to the Adsorption Mechanism, *Soil Sci. Soc. Am. J.*, **37(6)**: 863-868(1973).